Supplement of Atmos. Chem. Phys., 25, 18409–18429, 2025
https://doi.org/10.5194/acp-25-18409-2025-supplement

Atmospheric Chemistry and Physics Open Access

Supplement of

The role of aerosols and meteorological conditions in shaping cloud droplet development in New Mexico summer deep-convective systems

Huihui Wu et al.

Correspondence to: Hugh Coe (hugh.coe@manchester.ac.uk)

S1 Representation of entrainment in bin-microphysics parcel model

In this study, two types of entrainment processes are considered: homogeneous and inhomogeneous mixing. For homogeneous mixing, entrained subsaturated air uniformly mixes with and dilutes the cloud parcel, leading to a uniform reduction in droplet size. When humidity decreases sufficiently to induce droplet evaporation, the released aerosol particles may reactivate. These processes are implemented by including additional formulations in the solver routine that are passed to a variable-coefficient ordinary differential equation (VODE) solver. The related formulations are described in Pruppacher and Klett (2010, chapter 12). In brief, we assume a "jet" parcel, which allows entrainment to occur through the front interface of the plume. For a jet parcel with mass (m), density (ρ), radius (R_j) and vertical velocity (W), entrainment is described in terms of a change in mass flux $F_m = \pi R_j^2 \rho W$ along the vertical plume axis. The change in mass flux over a vertical distance Δz is expressed as $\Delta z(\mathrm{d}F_m/\mathrm{d}z)$, from which $\mathrm{d}F_m = 2\pi R_j \rho W \, \mathrm{d}R_j$. The entrainment rate for a jet (μ_j) is therefore

$$\mu_j = \frac{1}{F_m} \frac{\mathrm{d}F_m}{\mathrm{d}z} = \frac{C}{R_j} \tag{S1}$$

where C is the important entrainment parameter, which is set as 0.2 based on previous laboratory studies. Entrainment will cause the parcel volume to increase with time. The parcel acceleration is calculated by considering the buoyancy and reaction of the surrounding air:

$$\frac{\mathrm{d}W}{\mathrm{d}t} = \frac{\mathrm{g}}{1+\gamma} \left(\frac{T - T'}{T'} - w_L \right) - \frac{\mu_j}{1+\gamma} W^2 \tag{S2}$$

where $\gamma \approx 0.5$, g is the acceleration due to gravity ($\mathrm{g} \approx 9.80665$ m s^{-2}), w_L is the liquid water mixing ratio, T is the temperature of air parcel, and T' is the ambient temperature of the surrounding air. For a jet parcel, we can also relate the growth of the radius to the entrainment rate μ_j according to

$$\frac{\mathrm{d}\ln R_j}{\mathrm{d}t} = \frac{1}{2} \left[\mu_j W - \frac{\mathrm{d}\ln\rho}{\mathrm{d}t} - \frac{\mathrm{d}\ln W}{\mathrm{d}t} \right] \tag{S3}$$

which represents parcel dilution, expansion, and the conservation of mass flux, with $\frac{\mathrm{d}\rho}{\mathrm{d}t}$ expressed in terms of pressure and temperature derivatives using the ideal gas law. The condensed water is related to the water vapour mixing ratio (w_v), through an obvious statement of water conservation, this leads to

$$\frac{dw_v}{dt} = -\frac{dw_L}{dt} - \mu_j (w_v - w_v' + w_L) W \tag{S4}$$

Where w_L is the liquid water mixing ratio and w_v' is the ambient water vapour mixing ratio of the surrounding air. For the settings of aerosols, we initially set a number size distribution of dry aerosol particles ($n'_{AP,a}$) with mass (m'_{AP}), where $n_{AP,a}(m_{AP})$ is the number distribution of unactivated drops inside the air parcel at a time t. The $n_{AP,a}(m_{AP})$ changes are due to (1) entrainment of additional aerosol particles from the environmental air, (2) the activation of some of the aerosol particles to drops, and (3) drops which by evaporation become deactivated particles again. These changes are considered in simulations, which are expressed by

$$\frac{\partial n_{AP,a}(m_{AP})}{\partial t} = -\mu_j W\left[n_{AP,a}(m_{AP}) - n'_{AP,a}(m_{AP})\right] + \left.\frac{\partial n_{AP,a}(m_{AP})}{\partial t}\right|_{\text{activated/deactivated}} \quad \text{(S5)}$$

For inhomogeneous mixing, entrained subsaturated air remains in localized pockets rather than mixing instantaneously, leading to the evaporation of some droplets while others out of the pockets are unaffected. These processes are carried out outside the VODE solver, over a longer 10s timestep. The related formulations are the same as in the homogeneous mixing case (Eqs. S1-S5). For inhomogeneous mixing, the droplet number concentrations in each size bin are adjusted to conserve the parcel humidity, preventing a uniform reduction in droplet size as in the homogeneous mixing. When inhomogeneous mixing causes droplet evaporation, aerosol particles are released back into the discrete packets of subsaturated air, within the parcel, which may become re-activated later.

Table S1. Summary of the data availability for aerosol and cloud instruments.

Flight ID	Date	AMS	SP2	SMPS	PCASP	CPC	CDP
C297	16/07/2022	N	Y	N	Y	Y	Y
C298	19/07/2022	N	Y	Y	Y	Y	Y
C299	20/07/2022	Y	Y	Y	Y	Y	Y
C300	22/07/2022	Y	Y	Y	Y	Y	Y
C301	23/07/2022	Y	Y	N	Y	Y	Y
C302	24/07/2022	Y	Y	Y	Y	Y	Y
C303	25/07/2022	Y	Y	Y	Y	Y	Y
C304	26/07/2022	(Y)	Y	Y	Y	Y	Y
C305	27/07/2022	Y	Y	Y	Y	Y	Y
C306	29/07/2022	Y	Y	Y	Y	Y	Y
C307	30/07/2022	Y	Y	Y	Y	Y	Y
C308	31/07/2022	Y	N	Y	Y	Y	Y
C309	01/08/2022	Y	Y	Y	Y	Y	Y
C310	02/08/2022	Y	Y	Y	Y	Y	Y
C311	03/08/2022	N	Y	Y	Y	Y	Y
C312	04/08/2022	N	Y	Y	Y	Y	Y
C313	06/08/2022	Y	Y	(Y)	Y	Y	Y
C314	07/08/2022	(Y)	(Y)	Y	Y	Y	Y
C315	08/08/2022	N	N	Y	Y	Y	Y

Note: N represent unavailable data, Y represent available data, (Y) represent not completely available data.

Table S2. Summary of cloud properties in the lowest measured clouds and below-cloud aerosols.

Flight ID	Date	below-cloud N_a, cm^{-3}	N_d, cm^{-3}	LWC, $g\ m^{-3}$	R_e, μm	Approximate Distance (m)
C298	19/07/2022	632±172 (highest: 1439)	722±230 (highest: 1045)	0.08±0.02	3.2±0.2	−30
C299	20/07/2022	533±129 (1472)	609±345 (1055)	0.08±0.05	3.3±0.2	−150
C300	22/07/2022	636±200 (1490)	543±342 (1015)	0.13±0.09	4.2±0.1	−90
C301	23/07/2022	556±157 (1198)	521±290 (777)	0.17±0.09	4.6±0.0	120
C303	25/07/2022	770±86 (1070)	487±163 (663)	0.81±0.43	8.1±0.3	500
C304	26/07/2022	412±49 (508)	269±202 (593)	0.40±0.36	8.1±0.5	540
C305	27/07/2022	619±188 (1202)	881±333 (1292)	0.39±0.17	5.1±0.3	20
C306	29/07/2022	707±134 (1081)	509±292 (1030)	0.72±0.47	7.6±0.6	400
C307	30/07/2022	526±59 (665)	500±233 (860)	0.87±0.52	8.0±0.3	600
C308	31/07/2022	298±109 (531)	320±134 (525)	0.45±0.28	7.5±0.9	500
C309	01/08/2022	555±95 (892)	540±267 (932)	0.31±0.19	5.6±0.4	280
C310	02/08/2022	521±155 (1216)	669±375 (974)	0.16±0.10	4.1±0.2	−40
C312	04/08/2022	859±235 (1239)	591±248 (1018)	0.67±0.43	6.8±0.6	120
C313	06/08/2022	642±177 (962)	525±247 (969)	0.21±0.15	4.9±0.9	10
C314	07/08/2022	795±166 (1097)	727±340 (1025)	0.22±0.09	4.7±0.5	−230

Note: The distances are approximate distances between the lowest measured cloud layers and the lifting condensation level (LCL) heights.

Table S3. Experimental conditions used for case studies.

Exp.	Initial T (K)	Initial P (hpa)	RH (%)	kappa	Size mode	Initial updraft velocity (m/s)	Initial parcel radius
Period 1-C300 case	277	576.45	95	0.27	Mode1	2.5	1000
Period 2-C303 case	282	650.17	95	0.41	Mode2	2.5	1000

Note: T represents temperature, P represents pressure, and RH represents relative humidity. The setup of initial T, P, and aerosol characteristics (kappa and size modes) are selected from two flights (C300 and C303). Aerosol size distributions were averaged over near cloud-base straight and level runs. The size modes are displayed in Fig. S7. The initial T and P were averaged within 200 m below the LCL height.

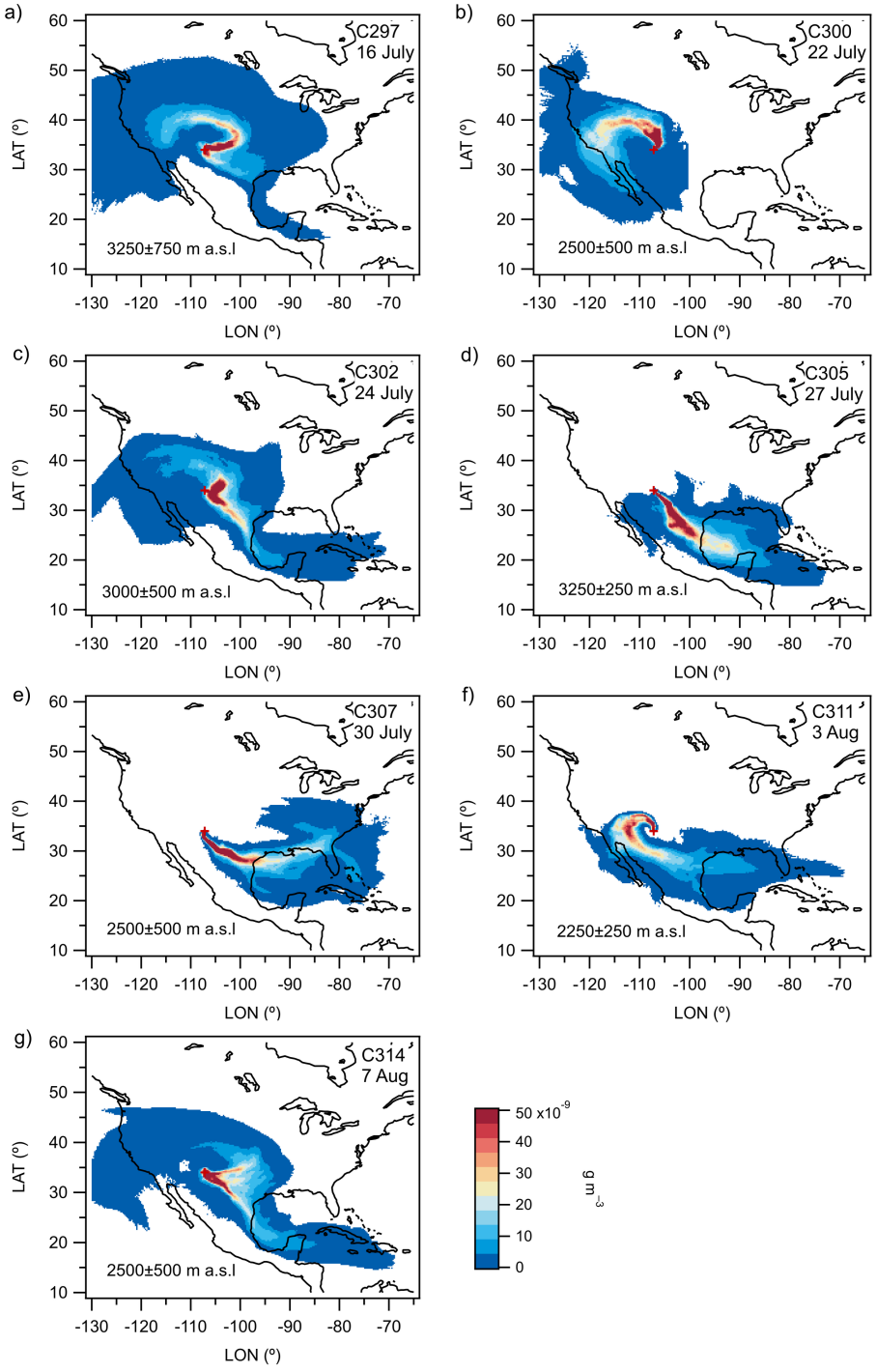

Figure S1. Examples of backward-dispersion fields from selected flight simulations, illustrating different and representative horizontal footprints of original air parcels transported over the past six days before reaching the sampling area during the campaign. The corresponding flight numbers and dates are indicated in the upper-right corner of each panel. The release area is marked with a red cross. The release height ranges are indicated in the lower-left corner of each panel.

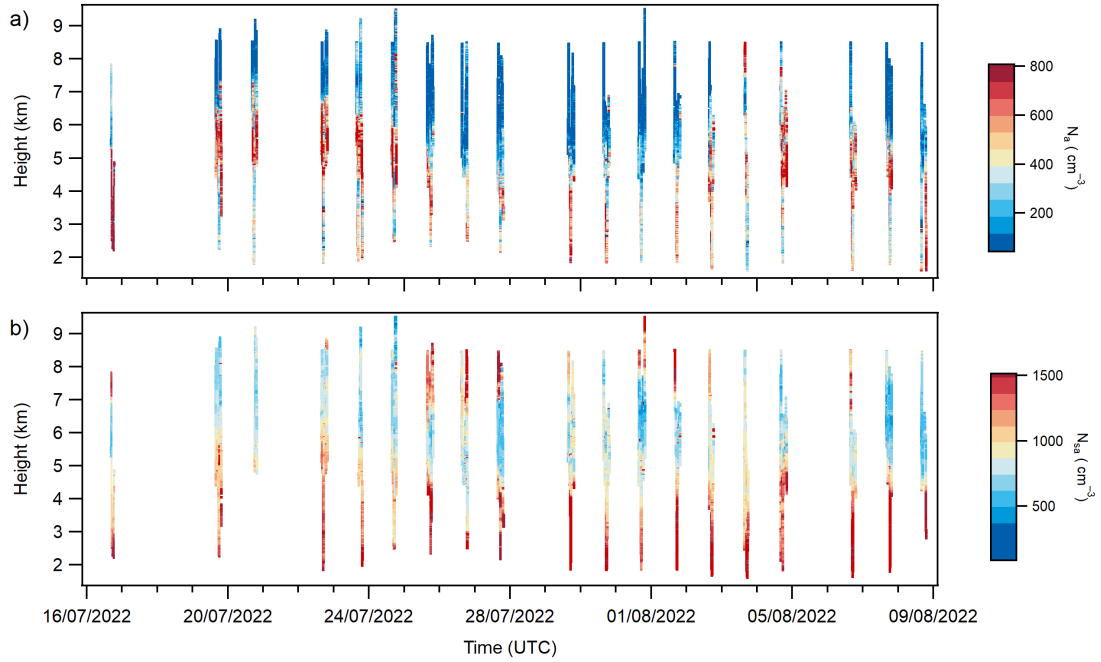

Figure S2. Vertical profiles of out-of-cloud (a) aerosol number concentrations in the accumulation mode (N_a, 0.1 – 3 µm) from PCASP measurements and (b) submicron aerosol number concentrations (N_{sa}, 2.5 nm to 1 µm) from CPC measurements, for each flight.

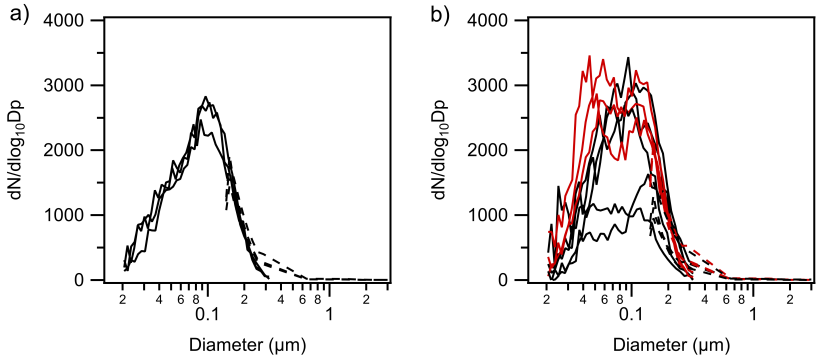

Figure S3. Average size distributions over near cloud-base straight and level runs for each single flight in (a) Period 1 and (b) Period 2. The solid lines represent results from SMPS, and the dashed lines represent results from PCASP. The red lines in (b) highlight the bimodal size distributions with a distinct minimum between the two modes.

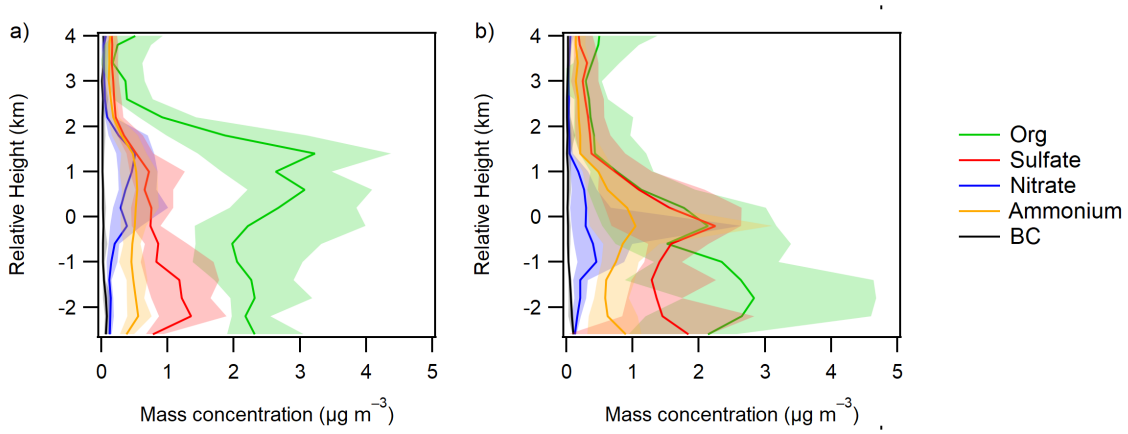

Figure S4. Average vertical profiles of mass concentrations of different chemical components out-of-cloud in (a) Period 1 and (b) Period 2. The lines and shades represent mean values and standard deviations. The y-axis is the relative height with respect to the LCL height.

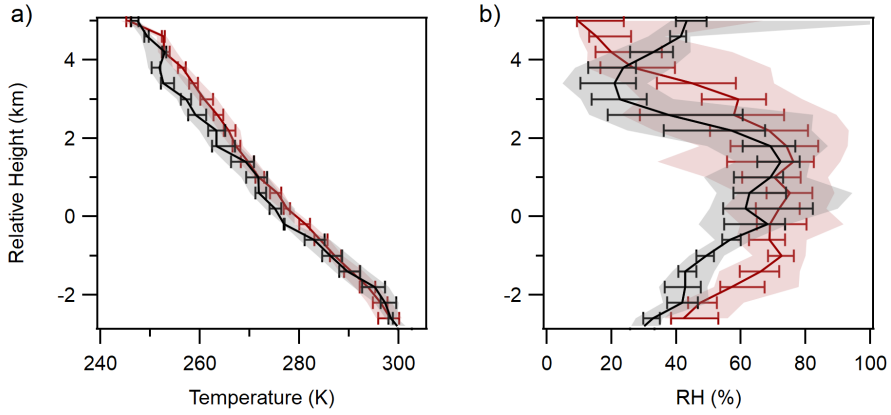

Figure S5. Vertical profiles of (a) Temperature (K) and (b) RH (%). Black values represent results from Period 1, and red values represent results from Period 2. The lines, bars and shades represent medians, 25 to 75 percentiles, and 10 to 90 percentiles. The y-axis is the relative height with respect to the LCL height.

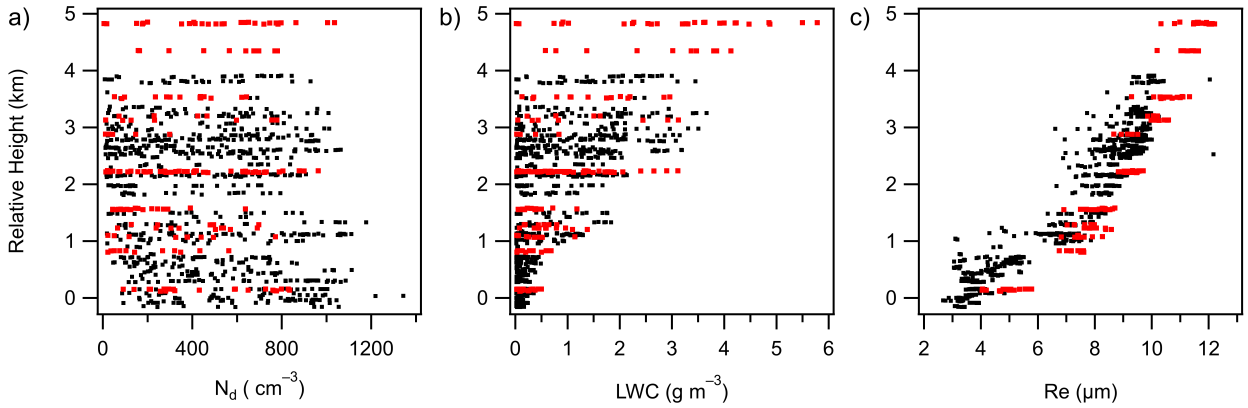

Figure S6. Vertical profiles of (a) cloud droplet number concentration (N_d, cm^{-3}), (b) liquid water content (LWC, g m^{-3}), and (c) effective radius (R_e, μm) for Period 1 earlier flights (black, C298-C300) and C301 (red). The dots represent 1-hz measurements. The y-axis is the relative height with respect to the LCL height.

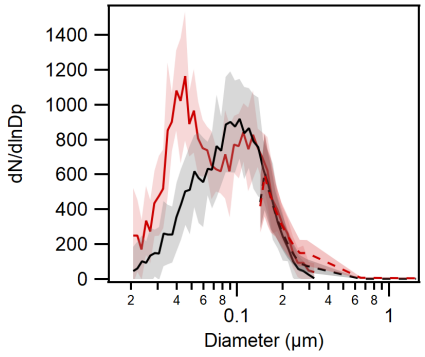

75

Figure S7. Aerosol size distributions (lines: mean values; shades: standard deviations) for the Period 1-C300 case (Mode 1, black) and the Period 2-C303 case (Mode 2, red) for bin microphysics parcel model simulations. The solid lines represent mean values from SMPS, and the dashed lines represent mean values from PCASP. It is noted that, for consistency with the model, the size distribution is expressed in "dN/dlnDp vs. Dp", and the unit of dN is expressed in "kg^{-1}".

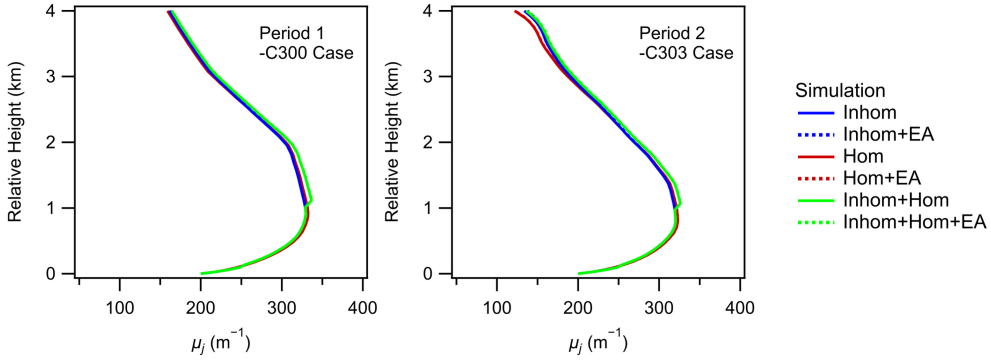

80

Figure S8. Vertical profiles of simulated μ_j (m^{-1}) for the Period 1-C300 case (left) and the Period 2-C303 case (right). The y-axis is the relative height with respect to the LCL height.

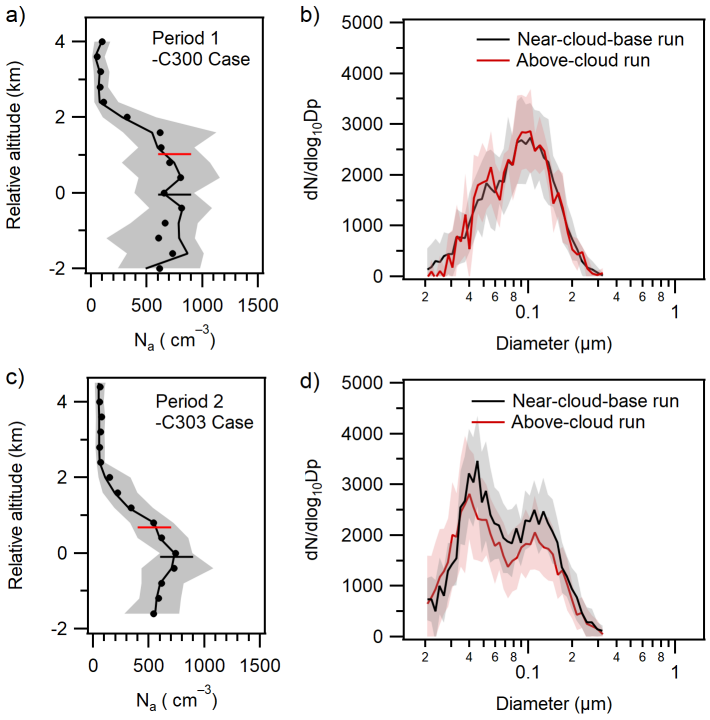

Figure S9. (a, c) Vertical profiles of out-of-cloud N_a for (a) the Period 1 case (C300) and (c) the Period 1 case (C303). The lines, dots and shades represent median, mean, and 10 to 90 percentiles. The black and red horizontal lines represent the heights of straight-and-level runs near the cloud base and above the cloud, respectively. The y-axis is the relative height with respect to the LCL height. (b, d) Average aerosol size distributions during straight-and-level runs near the cloud base (black) and above the cloud (red) for (b) the Period 1 case (C300) and (d) the Period 1 case (C303). Lines and shades represent mean values and standard deviations.

References

Pruppacher, H. R. and Klett, J. D.: Microphysics of Clouds and Precipitation, in: 2nd Edn., Springer, Dordrecht, https://doi.org/10.1007/978-0-306-48100-0, 2010.